

HiSST: 4th International Conference on High-Speed Vehicle Science Technology 22 -26 September 2025, Tours, France



Numerical Investigation of Scramjet Combustor Using Hydrogen Fuel: Comparison of Combustion Models

Si-Yoon Kang¹, Jae-Eun Kim¹ and Jeong-Yeol Choi²

Abstract

Supersonic combustion ramjet (scramjet) engines represent a key propulsion technology for high-speed atmospheric flight, where efficient fuel injection and flame stabilization remain critical challenges. In this study, we conduct a numerical analysis of a hydrogen-fueled scramjet combustor, focusing on the impact of different combustion models on flow characteristics and overall performance. To achieve computational efficiency while maintaining accuracy, Reynolds-Averaged Navier-Stokes (RANS) simulations were performed. Two turbulent-combustion models, including laminar chemistry and Partially Stirred Reactor (PaSR), were systematically compared. The numerical results were validated against available experimental data to assess the predictive ability of each model in capturing key phenomena such as ignition, flame stabilization, and thermal choking. To achieve this, this study aims to select an appropriate combustion model that can objectively evaluate and enhance the reliability of numerical predictions through thorough comparisons with previously validated scramjet cases. This study aims to provide valuable insights for the development of computationally efficient and accurate prediction tools. This will advance the design and optimization of future scramjet propulsion systems.

Keywords: High-speed vehicle, Hydrogen, Scramiet, Supersonic Combustion, Combustion Model

1. Introduction

With the rapid advancement of hypersonic flight technologies and reusable space launch systems, the scramjet engine has emerged as a key propulsion system for sustained flight at Mach 5 and beyond [1-3]. Unlike conventional gas turbine engines, scramjets rely on air compression through high-speed inlet flow rather than mechanical compressors, enabling superior thermodynamic efficiency. However, ensuring stable combustion under supersonic flow conditions and optimizing combustion efficiency remain significant technical challenges. One of the most critical issues in scramjet engines is fuel-air mixing, which directly impacts the engine's combustion performance. Given the extremely short residence time of air entering the combustor, typically measured in milliseconds, supersonic combustors have undergone extensive experimental and numerical research to overcome this issue.

Computational fluid dynamics (CFD) has been extensively used to analyze and optimize scramjet combustors, with Reynolds-Averaged Navier-Stokes (RANS) simulation being widely applied for turbulent-combustion model [4]. Despite the increasing use of these models, the optimal selection of a combustion model for supersonic turbulent combustion remains an open research problem. Previous studies have shown that the choice of combustion model significantly affects ignition delay, flame propagation speed, and combustion efficiency, necessitating a systematic comparative analysis.

In hydrogen-fueled scramjets, flow–combustion coupling has been quantified in HyShot-class transverse-jet/cavity flameholder studies, where ignition and flameholding mechanisms and their

-

¹ Graduate Research Assistant, Pusan National University, Busan 46241, Republic of Korea

² Professor, Pusan National University, Busan 46241, Republic of Korea, <u>aerochoi@pusan.ac.kr</u> (Corresponding)

pressure—spectral response were established; complementary Detached Eddy Simulation (DES) and RANS/LES of high-enthalpy transverse-jet ignition corroborate recirculation-assisted anchoring and the role of high-frequency instabilities [5-7]. Recent diagnostics that combine Dynamic Mode Decomposition (DMD), Short-Time Fourier Transform (STFT), and Chemical Explosive Mode Analysis (CEMA)—together with comprehensive reviews—show that unsteady combustion is governed by supersonic shear-layer mixing and ignition—extinction—reignition cycles, with the upstream pressure field exerting first-order control on combustor dynamics [8]. On the numerical side, high-resolution, low-dissipation schemes (oMLP/WENO/AUSMPW+) and contact-resolving approximate Riemann solvers, aided by reduced-Jacobian treatments, have improved predictive fidelity for scramjet and coaxial supersonic flames [9-12]. In parallel, work on ram/detonative propulsion and scram-accelerators has clarified shock—reaction coupling, thermal choking, and start-up behavior, supplying canonical boundary conditions and validation cases for high-speed combustors [13-15]. These advances—together with cross-validated RANS/LES—experiment studies on HyShot model combustors and structured sensitivity surveys over fuel, operating conditions, and combustion models—motivate the modeling/grid strategy and validation metrics adopted here [16].

This study aims to numerically analyze a hydrogen-fueled scramjet combustor by comparing various combustion models and assessing their impact on combustion characteristics and overall performance. The research is currently ongoing, and this paper presents the overarching objectives, methodology, and preliminary findings, providing insights into the current progress of the study.

2. Methodology & Preliminary Analysis

2.1. Navier-Stokes equations for chemical reacting flow

In this study, for the analysis of supersonic compressible reactive flow fields, the chemical species conservation equations, the Navier-Stokes equations, and the energy conservation equation, which are fully coupled to flow and chemical reactions, can be reorganized into conservation vector equations as follows [17, 18]. Here, if $\alpha = 0$, the governing equation is for two-dimensional flow, and if $\alpha = 1$, the governing equation is for an axisymmetric coordinate system. The specific expressions for each vector are as follows.

$$\frac{\partial \mathbf{Q}}{\partial t_f} + \frac{\partial \mathbf{F}}{\partial x} + \frac{\partial \mathbf{G}}{\partial y} = \frac{\partial \mathbf{F_v}}{\partial x} + \frac{\partial \mathbf{G_v}}{\partial y} \tag{1}$$

$$\mathbf{Q} = \begin{bmatrix} \rho_k \\ \rho u \\ \rho v \\ e \\ \rho k \\ \rho \omega \end{bmatrix}, \mathbf{F} = \begin{bmatrix} \rho_k u \\ \rho u^2 + p \\ \rho u v \\ (e+p)u \\ \rho u k \\ \rho u \omega \end{bmatrix}, \mathbf{G} = \begin{bmatrix} \rho_k v \\ \rho u v \\ \rho v^2 + p \\ (e+p)v \\ \rho v k \\ \rho v \omega \end{bmatrix},$$
$$\begin{bmatrix} -\rho_k u_k^d \\ \tau_{xy} \end{bmatrix} \begin{bmatrix} -\rho_k v_k^d \\ \tau_{xy} \end{bmatrix}$$

$$\mathbf{F}_{\mathbf{v}} = \begin{bmatrix} -\rho_{k} u_{k}^{d} \\ \tau_{xx} \\ \tau_{xy} \\ \beta_{x} \\ \underline{\mu_{k} \partial k} \\ \frac{\mu_{\omega} \partial \omega}{\partial x} \end{bmatrix}, \mathbf{G}_{\mathbf{v}} = \begin{bmatrix} -\rho_{k} v_{k}^{d} \\ \tau_{xy} \\ \tau_{yy} \\ \beta_{y} \\ \underline{\mu_{k} \partial k} \\ \frac{\partial y}{\partial y} \end{bmatrix}$$
(2)

where, the conserved variable vector \mathbf{Q} , the convective flux vectors \mathbf{F} and \mathbf{G} , the viscous flux vectors $\mathbf{F}_{\mathbf{v}}$ and $\mathbf{G}_{\mathbf{v}}$, and the computational time t in the fluid are given. Here, ρ and ρ_k are the densities of the

mixture and each chemical species, respectively, while u_k^d , v_k^d are the diffusion rates of each chemical species. All working fluids in this study are gaseous phases and operate under subcritical conditions.

The convective flux term is discretized using the Roe scheme, the MUSCL method was used for high-order spatial accuracy, and the β -minmod limiter was used to preserve the TVD property. For the viscous flux term, a second-order accurate central difference method was used. Time integration was performed using the LU-SGS implicit method. This numerical framework has been utilized not only to investigate the underlying intricate physics of scramjet combustor [19-26], but also to study the ram accelerators and bleed-based flows [27-30], shock-induced combustion [31-35]. Additionally, it has been employed in the design process of Rocket-Based Combined Cycle (RBCC) engines [36, 37].

2.2. Turbulence Modeling

For turbulence modelling, this study used Menter's two-equation $k-\omega$ SST model [38]. For an economical and efficient approach, we solved the Reynolds-Averaged Navier–Stokes (RANS) model, which models all scales of turbulence. The model blends Wilcox $k-\omega$ (near wall) [39] with a transformed $k-\varepsilon$ behaviour (free-stream) [40] via Menter's blending functions, providing robust separation prediction and improved sensitivity in strong convective-pressure-gradient regions typical of cavity-stabilized scramjet combustors with transverse injection and shock—shear interactions. Turbulent Prandtl and Schmidt numbers were set to 0.72 and 0.7, respectively.

2.3. Chemistry Modeling

High-enthalpy combustion of air and hydrogen is modeled using the Jachimowski's detailed laminar chemical mechanism for hydrogen/oxygen [41]. Jachimowski's detailed laminar chemical mechanism consists of 9 chemical species including H, H₂, O, O₂, H₂O, OH, HO₂, H₂O₂, N₂ and 19 reaction steps.

Table 1 Jachimowski's hydrogen/oxygen detailed chemical mechanism [41]

Table 1 Jacininovski s flydrogeri, oxygeri actalica chemical methanism [1]				
#	Reaction step	A_r	Br	E_r^*
1	$H_2 + O_2 \leftrightarrow HO_2 + H$	1.00×10 ¹⁴	0.00	56,000
2	$H + O_2 \leftrightarrow OH + O$	2.60×10 ¹⁴	0.00	16,800
3	$O + H_2 \leftrightarrow OH + H$	1.80×10^{10}	1.00	8,900
4	$OH + H_2 \leftrightarrow H_2O + H$	2.20×10^{13}	0.00	5,150
5	$OH + OH \leftrightarrow H_2O + O$	6.30×10^{12}	0.00	1,090
6	$H + OH + M \leftrightarrow H_2O + M$	2.20×10^{22}	-2.00	0
7	$H + H + M \leftrightarrow H_2 + M$	6.40×10^{17}	-1.00	0
8	$H + O + M \leftrightarrow OH + M$	6.00×10^{16}	-0.60	0
9	$H + O_2 + M \leftrightarrow HO_2 + M$	2.10×10^{15}	0.00	-1,000
10	$HO_2 + H \leftrightarrow OH + OH$	1.40×10^{14}	0.00	1,080
11	$HO_2 + H \leftrightarrow H_2O + O$	1.00×10^{13}	0.00	1,080
12	$HO_2 + O \leftrightarrow O_2 + OH$	1.50×10^{13}	0.00	950
13	$HO_2 + OH \leftrightarrow H_2O + O_2$	8.00×10^{12}	0.00	0
14	$HO_2 + HO_2 \leftrightarrow H_2O_2 + O_2$	2.00×10^{12}	0.00	0
15	$H + H_2O_2 \leftrightarrow H_2 + HO_2$	1.40×10^{12}	0.00	3,600
16	$O + H_2O_2 \leftrightarrow OH + HO_2$	1.40×10^{13}	0.00	6,400
17	$OH + H_2O_2 \leftrightarrow H_2O + HO_2$	6.10×10^{12}	0.00	1,430
18	$H_2O_2 + M \leftrightarrow OH + OH + M$	1.20×10^{17}	0.00	45,600
19	$O + O + M \leftrightarrow O_2 + M$	6.00×10^{13}	0.00	-1,800
	Third body efficiencies relative to N ₂			
6	$H + OH \leftrightarrow H_2O + M$	$H_2O = 6.00$	H ₂ =	= 1.00
7	$H + H + M \leftrightarrow H_2 + M$	$H_2O = 6.00$	$H_2 = 2.00$	
8	$H + O + M \leftrightarrow OH + M$	$H_2O = 5.00$	H ₂ =	= 1.00
9	$H + O_2 + M \leftrightarrow HO_2 + M$	$H_2O = 16.00$	H ₂ =	= 2.00
19	$H_2O_2 + M \leftrightarrow OH + OH + M$	$H_2O = 15.00$	H ₂ =	= 1.00
	$k_{fr}=A_rT^{Br}e^{-rac{E_r^*}{RT}}$			
	icr			

where A_r is the pre-exponential factor, B_r is non dimensional, and E_r^* is the activation temperature in Table 1. The forward chemical reaction rate constant, k_{fr} , for the r-th chemical reaction step can be calculated in Arrhenius form. Backwards rates are computed using chemical equilibrium. The reaction rate of each chemical species is shown below.

$$\dot{\omega}_{s} = M_{k} \sum_{r=1}^{N_{r}} \left(v_{k,r}^{"} - v_{k,r}^{"} \right) \left[k_{fr} \prod_{k=1}^{N} \left(\frac{\rho_{k}}{M_{k}} \right)^{v_{k,r}^{"}} - k_{br} \prod_{k=1}^{N} \left(\frac{\rho_{k}}{M_{k}} \right)^{v_{k,r}^{"}} \right]$$
(3)

2.4. Theoretical formula of PaSR

Some simulations presented here are based on laminar chemistry assumptions, which do not model sub-grid turbulent chemical interactions, and all reaction rates are evaluated using resolved flow quantities. The remaining simulations use a partially stirred reactor model (PaSR) for sub-grid turbulent chemical interactions. The model used here closely follows the work of Kartha et al. [42] and Peterson et al. [43]. In the partially stirred reactor model, reactions are assumed to occur only in a portion of the volume of a given cell. The filtered reaction rates are evaluated as follows:

$$\overline{\dot{\omega}_{s}(\rho_{s},T)} \approx \dot{\omega}_{s}(\gamma^{*}\widetilde{\rho_{s}},\widetilde{T}) \approx \gamma^{*}\dot{\omega}_{s}(\widetilde{\rho_{s}},\widetilde{T}) \tag{4}$$

where $\dot{\omega}_s$ is the reaction rate of species, ρ_s is the density of species, T is the temperature, and γ^* is the microscale volume fraction. The overbar represents filtering, and the tilde represents Favre-filtering. In many partially stirred reactor model formulas, γ^* is multiplied by the overall reaction rate rather than the species density. The microscale volume fraction is given below.

$$\gamma^* = \frac{t_c}{\max\left(t_c, \frac{Re_{\Delta} - 1}{Re_{\Delta}} t_s\right)} \text{ where } Re_{\Delta} = \frac{\max\left(u'_{SGS}, \frac{v}{\Delta}\right) \Delta}{v}$$
 (5)

where t_c is the characteristic time scale of chemistry, t_s is the characteristic time scale of the sub-grid velocity, and Re_{Λ} is a factor that reduces the value to 1.0 in the laminar flow. Here, SGS represents the sub-grid velocity fluctuation and viscosity. The characteristic time scale of chemistry and the characteristic time scale of the sub-grid velocity are defined as:

$$\frac{1}{t_c} \equiv \frac{\max(\|\widetilde{\omega}_{lam}^+\|, \|\widetilde{\omega}_{lam}^-\|)}{\bar{\rho}} \qquad (6)$$

$$t_s = \frac{\Delta}{\max(u_{SGS'}^{\frac{v}{\Delta}})} \qquad (7)$$

$$t_{s} = \frac{\Delta}{\max\left(u_{SGS}', \frac{v}{\Delta}\right)} \tag{7}$$

2.5. Test cases

2.5.1. Burrows and Kurkov's combustor

The Burrows and Kurkov case was first analysed, which has a configuration shown in Fig. 1. In the experiment, hydrogen was injected into a contaminated air stream. A water-cooled thermocouple probe was used to measure the total temperature, and a water-cooled Pitot probe was used to measure the pressure. A pressure port was located at the leading edge of the probe. A miniature rolled thermocouple and a miniature Pitot pressure tube were used in the boundary layer and the low-temperature hydrogen-rich mixing region. Finally, two similar water-cooled sampling probes were installed for gas sampling and indirect temperature measurements. The experimental profiles of temperature, Mach number, H₂, and H₂O mole fraction at the outlet were used to validate the CFD simulation results.

The air entering the combustor from the left is assumed to be vitiated air at Mach 2.44. The temperature and pressure are 1,270 K and 0.1 MPa, respectively. Hydrogen is injected into the combustor at Mach 1.0 and pressures of 254 K and 0.1 MPa, respectively. The viscous wall condition is employed for the boundary condition at the wall, and the temperature is 298 K. The outflow boundary condition is used in the form of pressure extrapolation in the outlet region. The computational domain uses the same number of grids as those provided by NASA. However, the detailed chemical reaction mechanism used is different, and as mentioned above, Jachimowski's reaction mechanism is applied in this study.

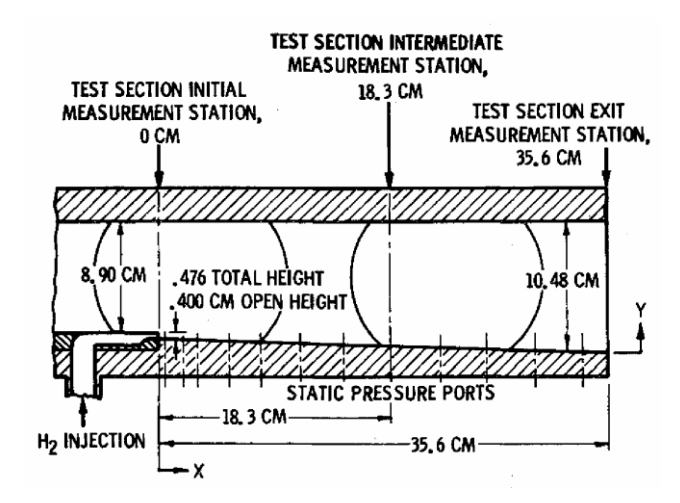


Figure 1 Schematic of the geometry and experimental configuration of the Burrows and Kurkov's combustor [44]

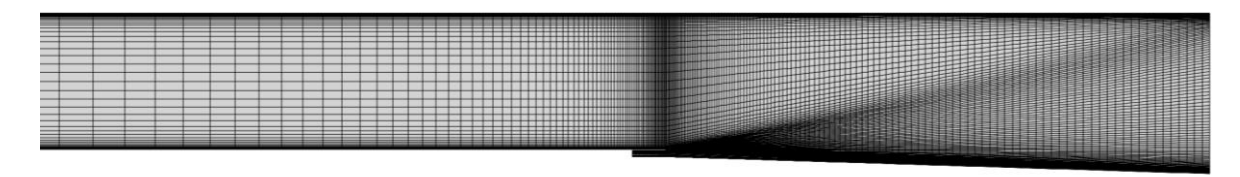


Figure 2 Computational domain of Burrows and Kurkov's combustor

2.5.2. DLR scramjet combustor

The DLR scramjet combustor proposed by Waidmann et al. [45] and Berglund et al. [46] uses hydrogen as fuel, injected through 15 holes parallel to the airflow. These holes are spaced 2.4 mm apart, have a diameter of 1 mm, and are angled at a 6° radius from the wedge central axis. The upper wall provides a 3° angular divergence to compensate for boundary layer growth. The combustor is 340 mm long, 40 mm wide, and has an inlet height of 50 mm. The DLR scramjet combustor uses a strut-based configuration to help address the ignition problems of typical scramjet engines. The flame holder is 32 mm long and 6 mm high. To reduce computational costs, a small region with only a single hole was maintained, assuming a two-dimensional domain, considering symmetric boundary conditions at the horizontal injection plane. No-slip boundary conditions were applied at the walls, and a flow-based far-field boundary condition was selected for the inlet.

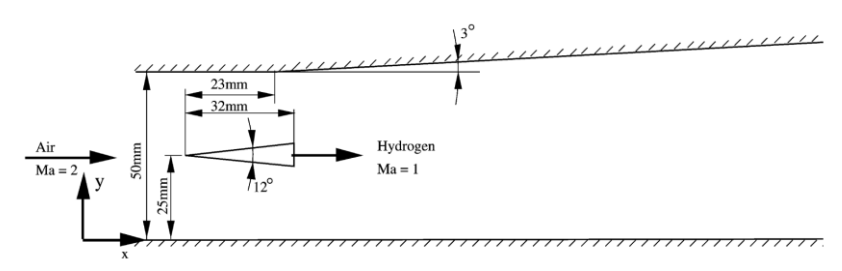


Figure 3 Schematic diagram of the DLR scramjet combustion chamber [47]



Figure 4 Computational domain of DLR scramjet combustion chamber

3. Results & discussion

3.1. Burrows and Kurkov's combustor

This study focuses on the numerical investigation of a hydrogen-fueled scramjet combustor, comparing different combustion models to evaluate their impact on combustion characteristics. The interaction between turbulence and chemical reactions plays a dominant role in supersonic combustion, making the selection of an appropriate combustion model crucial for optimizing performance. For the Burrows and Kurkov case, differences in ignition onset point were observed, as shown in Fig. 5. The top image in Fig. 5 shows the analysis results based on laminar chemistry, while the bottom image shows the analysis results using PaSR. Comparing this with the NASA-provided Burrows and Kurkov case analysis results, which show flame attachment at approximately 140 mm, the PaSR analysis results show a more accurate flame front location.

Figure 6 shows the experimental and simulated radial profiles of total temperature, Mach number, H_2O mole fraction, and H_2 mole fraction at the exit plane. Total temperature profiles provide similar quantitative results for both models, which are very similar to the experimental results. The Mach number plot confirms the formation of a boundary layer at the wall, and the difference from the experimental results is particularly noticeable at y = 20 mm, the peak total temperature region. Although there are quantitative errors in the H2O and H2 mole fractions, the trends are very similar.

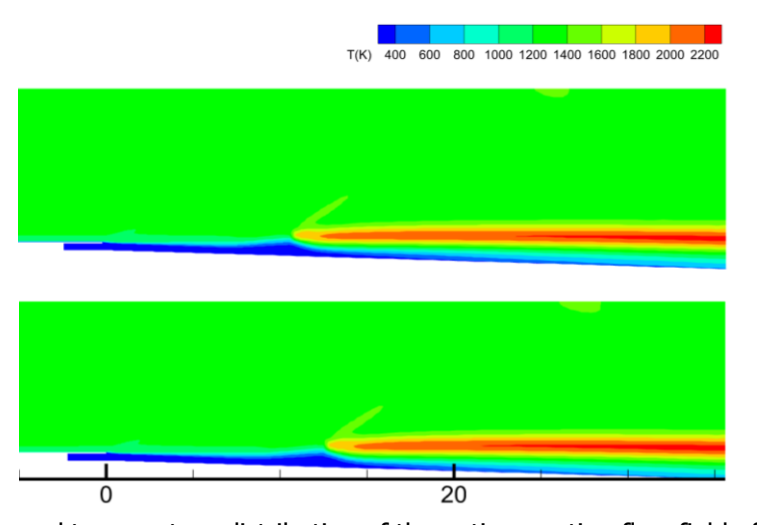


Figure 5 Time-averaged temperature distribution of the entire reaction flow field of the Burrows and Kurkov case (top) Laminar chemistry model, (bottom) PaSR model

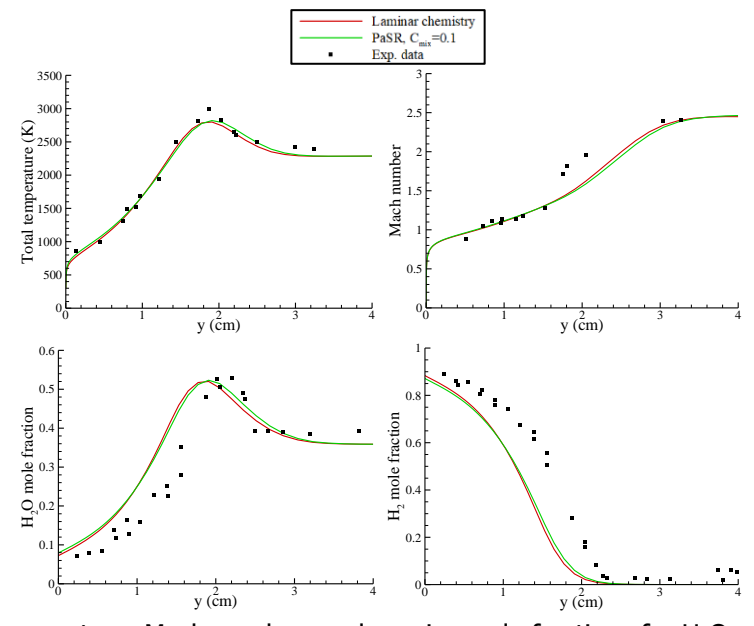


Figure 6 Total temperature, Mach number, and species mole fractions for H₂O and H₂ at the exit

3.2. DLR scramjet combustor

Figure 7 compares the shadow image extracted during the experiment with a numerical density gradient plot in the reacting flow field obtained from a laminar chemistry model. Both results demonstrate that combustion heat release expands the density gradient region. The shock wave locations and formations in the two figures are in good agreement. The supersonic airflow entering from the inlet region first collides with the tip of the wedge, forming an oblique shock wave that interacts with the boundary layer and is reflected by the upper and lower walls, thickening the boundary layer.

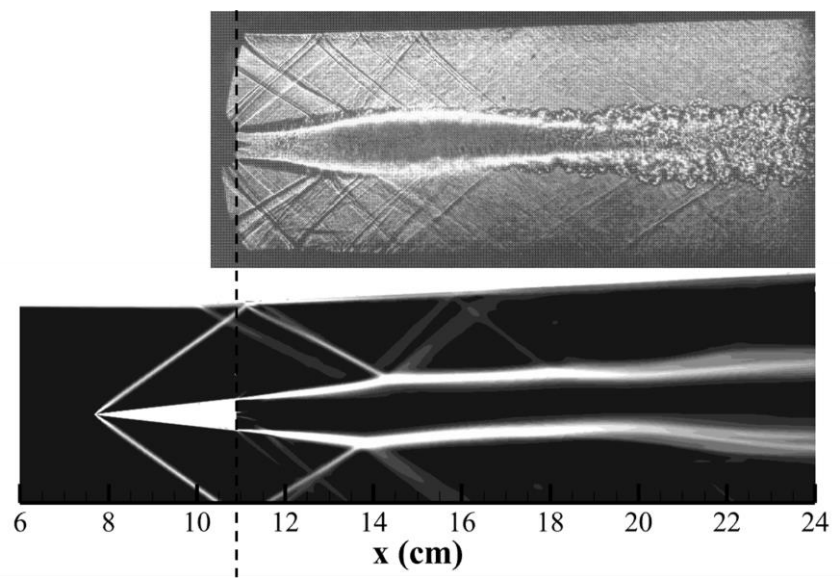


Figure 7 (top) Shadow image, (bottom) density gradient of reactive flow field of the DLR scramjet combustion chamber

Figure 8 compares the temperatures derived from laminar chemistry and PaSR at three different axial locations. At x=123 mm, the laminar chemistry model accurately predicts the temperature in the hydrogen jet region. In contrast, the temperature profile with the PaSR model is less accurate in the hydrogen jet region, but predicts the temperature in the upper shear layer more accurately. As mentioned earlier, the PaSR model results in a slight thickening of the flame, which can be seen in the x=170 mm region. In this region, the laminar chemistry model results show higher accuracy. The results in the x=278 mm region show a significant error for both models.

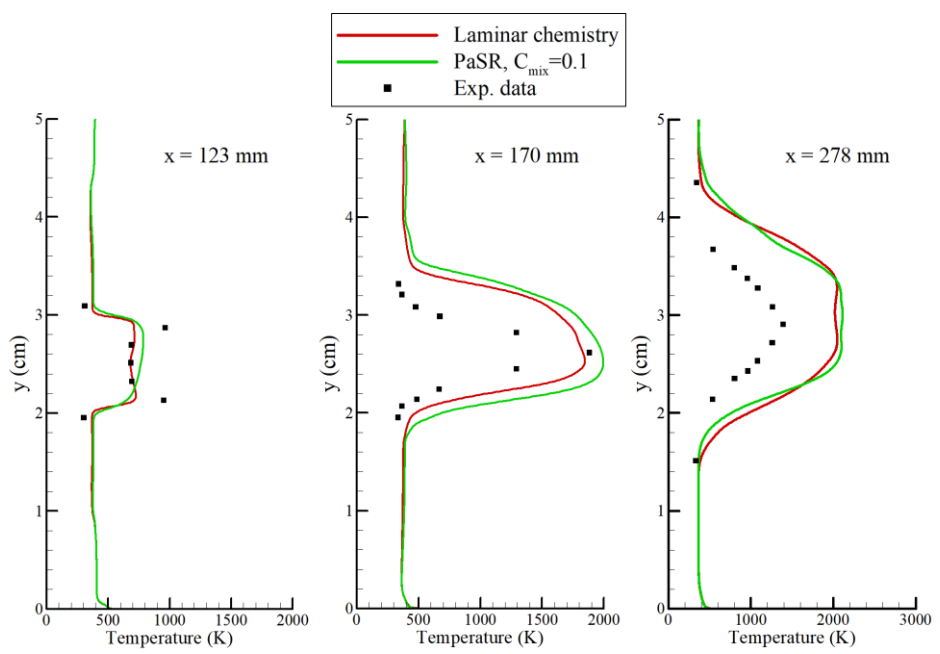


Figure 8 Experimental and simulated radial profiles of static temperature at three different axial locations (left) x = 12.3 cm, (middle) x = 17.0 cm, (right) x = 27.8 cm

Figure 9 shows the mass fraction distribution of OH. The left side is the laminar chemistry analysis result, and the right side is the PaSR model result. Unlike laminar chemistry, the PaSR model, which forms the combustion field by combining the chemical time scale and the sub-grid velocity time scale, shows a slight suppression of combustion in the shear layer, resulting in a slower chemical reaction. This is similar to the results in the Burrows and Kurkov case. This is because the reaction considering the mixing time scale increases the effective reaction time, further slowing the reaction in areas such as the flame anchoring point. This delayed combustion effect causes combustion to occur relatively downstream, thickening the reaction region and spreading the OH distribution more widely.

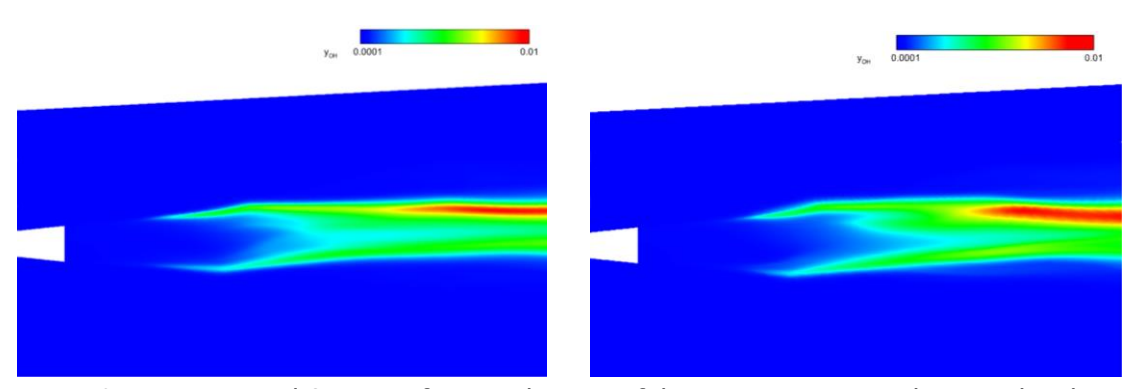


Figure 9 Time-averaged OH mass fraction diagram of the DLR scramjet combustion chamber (left) Laminar chemistry model, (right) PaSR model

4. Conclusion

This work numerically examined a hydrogen-fueled scramjet combustor with emphasis on how the choice of turbulent-combustion model alters the predicted flow physics and performance. Model predictions were compared against available experiments to assess fidelity in ignition, flame stabilization, and the onset of thermal choking. The principal findings are:

- 1. Predictive capability vs. robustness trade-off. Laminar chemistry can better expose kinetic-limited induction and localized ignition physics but is more sensitive to grid, inflow T_0 , and numerical dissipation near shocks. PaSR is more robust under design-space sweeps and maintains reasonable agreement with experiments when mixing time scales are chosen consistently with the k- ω SST field.
- 2. Computational efficiency with controlled accuracy.
 The third-order scheme within a RANS framework, combined with parallelization, delivered tractable turnaround times suitable for parametric studies, while preserving the main trends needed for early-stage design and screening.

Overall, the study shows that turbulent combustion model impacts scramjet performance predictions, and provides practical guidance for choosing between accuracy in ignition physics (laminar chemistry) and robust, design-oriented assessments (PaSR)—a balance essential for efficient design and optimization of future scramjet propulsion systems.

References

- 1. Gardner, A., Steelant, J., Paull, A., Hannemann, K.: Ground testing of the HyShot supersonic combustion flight experiment in HEG and comparison with flight data. 40th AIAA/ASME/SAE/ASEE Joint Propulsion Conference and Exhibit, 3345 (2004). https://doi.org/10.2514/6.2004-3345.
- 2. Ingenito, A., Bruno, C., Cecere, D.: LES of the HyShot scramjet combustor. 48th AIAA Aerospace Sciences Meeting Including the New Horizons Forum and Aerospace Exposition, 758 (2010). https://doi.org/10.2514/6.2010-758.
- 3. Sunami, T., Itoh, K., Satoh, K., Komuro, T.: Mach 8 ground tests of the hypermixer scramjet for HyShot-IV flight experiment. 14th AIAA/AHI Space Planes and Hypersonic Systems and Technologies Conference, 8062 (2006). https://doi.org/10.2514/6.2006-8062.
- 4. You, Y., Luedeke, H., Hannemann, K.: Injection and mixing in a scramjet combustor: DES and RANS studies. Proc. Combust. Inst. 34, 2083-2092 (2013). https://doi.org/10.1016/j.proci.2012.10.001.
- 5. Won, S.-H., Jeung, I.-S., Choi, J.-Y.: DES investigation of the ignition of hydrogen transverse jet into high enthalpy supersonic crossflow. 47th AIAA Aerospace Sciences Meeting including The New Horizons Forum and Aerospace Exposition, 1557 (2009). https://doi.org/10.2514/6.2009-1557.
- 6. Choi, J.-Y., Ma, F., Yang, V.: Dynamic Combustion Characteristics in Scramjet Combustors with Transverse Fuel Injection. 41st AIAA/ASME/SAE/ASEE Joint Propulsion Conference & Exhibit, (2012).
- 7. Won, S.-H., Jeung, I.-S., Choi, J.-Y.: Turbulent combustion characteristics in HyShot model combustor with transverse fuel injection. 43rd AIAA/ASME/SAE/ASEE Joint Propulsion Conference & Exhibit, 5427 (2007). https://doi.org/10.2514/6.2007-5427.
- 8. Jeong, S.-M., Choi, J.-Y.: Combined diagnostic analysis of dynamic combustion characteristics in a scramjet engine. Energies. 13, 4029 (2020). https://doi.org/10.3390/en13154029.
- 9. Vyasaprasath, K., Oh, S., Kim, K.-S., Choi, J.-Y.: Numerical studies of supersonic planar mixing and turbulent combustion using a detached eddy simulation (DES) model. Int. J. Aeronaut. Space Sci. 16, 560-570 (2015). http://dx.doi.org/10.5139/IJASS.2015.16.4.560.
- 10. Kim, S.D., Lee, B.J., Lee, H.J., Jeung, I.-S., Choi, J.-Y.: Realization of contact resolving approximate Riemann solvers for strong shock and expansion flows. Int. J. Numer. Methods Fluids. 62, 1107-1133 (2010). https://doi.org/10.1002/fld.2057.
- 11. Choi, J., Kim, K.H., Han, S.: High resolution numerical study on the coaxial supersonic turbulent flame structures. 50th AIAA/ASME/SAE/ASEE Joint Propulsion Conference, 3745 (2014). https://doi.org/10.2514/6.2014-3745.
- 12. Kim, S.-L., Choi, J.-Y., Jeung, I.-S., Park, Y.-H.: Application of approximate chemical Jacobians for constant volume reaction and shock-induced combustion. Appl. Numer. Math. 39, 87-104 (2001). https://doi.org/10.1016/S0168-9274(01)00054-X.
- 13. Cho, D.-R., Won, S.-H., Shin, J.-R., Choi, J.-Y.: Numerical study of three-dimensional detonation wave dynamics in a circular tube. Proc. Combust. Inst. 34, 1929-1937 (2013). https://doi.org/10.1016/j.proci.2012.08.003.
- 14. Ma, F., Choi, J.-Y., Yang, V.: Thrust chamber dynamics and propulsive performance of single-tube pulse detonation engines. J. Propul. Power. 21, 512-526 (2005). https://doi.org/10.2514/1.7393.
- 15. Choi, J.-Y., Jeung, I.-S., Yoon, Y.: Transient simulation of superdetonative mode initiation process in scram-accelerator. Symp. Combust. Proc., Elsevier, 2957-2963 (1996). https://doi.org/10.1016/S0082-0784(96)80138-X.
- 16. Choi, J.-Y., Unnikrishnan, U., Hwang, W.-S., Jeong, S.-M., Han, S.-H., Kim, K.H., Yang, V.: Effect of fuel temperature on flame characteristics of supersonic turbulent combustion. Fuel. 329, 125310 (2022). https://doi.org/10.1016/j.fuel.2022.125310.
- 17. Choi, J.-Y., Jeung, I.-S., Yoon, Y.: Computational fluid dynamics algorithms for unsteady shock-induced combustion, part 1: validation. AIAA journal. 38, 1179-1187 (2000). https://doi.org/10.2514/2.1112.
- 18. Choi, J.-Y., Jeung, I.-S., Yoon, Y.: Computational fluid dynamics algorithms for unsteady shock-induced combustion, part 2: comparison. AIAA journal. 38, 1188-1195 (2000). https://doi.org/10.2514/2.1087.
- 19. Choi, J.-Y., Ma, F., Yang, V.: Dynamic combustion characteristics in scramjet combustors with transverse fuel injection. 41st AIAA/ASME/SAE/ASEE Joint Propulsion Conference & Exhibit, 4428 (2005). https://doi.org/10.2514/6.2005-4428.

- 20. Choi, J.-Y., Ma, F., Yang, V., Won, S.-H., Jeung, I.-S.: Detached Eddy simulation of combustion dynamics in scramjet combustors. 43rd AIAA/ASME/SAE/ASEE Joint Propulsion Conference & Exhibit, 5027 (2007). https://doi.org/10.2514/6.2007-5027.
- 21. Choi, J., Noh, J., Byun, J.-R., Lim, J.-S., Togai, K., Yang, V.: Numerical investigation of combustion/shock-train interactions in a dual-mode scramjet engine. 17th AIAA International Space Planes and Hypersonic Systems and Technologies Conference, 2395 (2011). https://doi.org/10.2514/6.2011-2395.
- 22. Jeong, S.-M., Kim, J.-E., Lee, J.H., Choi, J.: Analysis on Flow-Field Characteristics of a Scramjet Combustor with respect to Equivalence Ratio using IDDES Simulation. AIAA SCITECH 2023 Forum, 2189 (2023). https://doi.org/10.2514/6.2023-2189.
- 23. Choi, J.-Y., Ma, F., Yang, V.: Combustion oscillations in a scramjet engine combustor with transverse fuel injection. Proc. Combust. Inst. 30, 2851-2858 (2005). https://doi.org/10.1016/j.proci.2004.08.250.
- 24. Jeong, S.-M., Han, H.-S., Sung, B.-K., Lee, E.S., Choi, J.: Numerical simulation of combustion instability in a direct-connect supersonic combustor. AIAA Propulsion and Energy 2021 Forum, 3535 (2021). https://doi.org/10.2514/6.2021-3535.
- 25. Jeong, S.-M., Lee, J.-H., Choi, J.-Y.: Numerical investigation of low-frequency instability and frequency shifting in a scramjet combustor. Proc. Combust. Inst. 39, 3107-3116 (2023). https://doi.org/10.1016/j.proci.2022.07.245.
- 26. Jeong, S.-M., Han, H.-S., Sung, B.-K., Kim, W., Choi, J.-Y.: Reactive flow dynamics of low-frequency instability in a scramjet combustor. Aerospace. 10, 932 (2023). https://doi.org/10.3390/aerospace10110932.
- 27. Choi, J.-Y., Jeung, I.-S., Yoon, Y.: Numerical study of scram accelerator starting characteristics. AIAA journal. 36, 1029-1038 (1998). https://doi.org/10.2514/2.476.
- 28. Choi, J.-Y., Jeung, I.-S., Yoon, Y.: Unsteady-state simulation of model ram accelerator in expansion tube. AIAA journal. 37, 537-543 (1999). https://doi.org/10.2514/2.770.
- 29. Choi, J.-Y., Shin, E., Kim, C.-K.: Numerical study of base-bleed projectile with external combustion. 41st AIAA/ASME/SAE/ASEE Joint Propulsion Conference & Exhibit, 4352 (2005). https://doi.org/10.2514/6.2005-4352.
- 30. Shin, E., Won, S., Cho, D.-R., Choi, J.-Y.: Hybrid RANS/LES study of base-bleed flows in supersonic mainstream. 15th AIAA International Space Planes and Hypersonic Systems and Technologies Conference, 2588 (2008). https://doi.org/10.2514/6.2008-2588.
- 31. Choi, J.-Y., Jeung, I.-S., Lee, S.: Dimensional analysis of the effect of flow conditions on shock-induced combustion. Symp. Combust. Proc., Elsevier, 2925-2932 (1996). https://doi.org/10.1016/S0082-0784(96)80134-2.
- 32. Choi, J.-Y., Jeung, I.-S., Yoon, Y.: Scaling effect of the combustion induced by shock-wave boundary-layer interaction in premixed gas. Symp. Combust. Proc., Elsevier, 2181-2188 (1998). https://doi.org/10.1016/S0082-0784(98)80067-2.
- 33. Kumar, P.P., Kim, K.-S., Oh, S., Choi, J.-Y.: Numerical comparison of hydrogen-air reaction mechanisms for unsteady shock-induced combustion applications. J. Mech. Sci. Technol. 29, 893-898 (2015). https://doi.org/10.1007/s12206-015-0202-2.
- 34. Pavalavanni, P.K., Sohn, C.H., Lee, B.J., Choi, J.-Y.: Revisiting unsteady shock-induced combustion with modern analysis techniques. Proc. Combust. Inst. 37, 3637-3644 (2019). https://doi.org/10.1016/j.proci.2018.07.094.
- 35. Pavalavanni, P.K., Jo, M.-S., Kim, J.-E., Choi, J.-Y.: Numerical study of unstable shock-induced combustion with different chemical kinetics and investigation of the instability using modal decomposition technique. Aerospace. 10, 292 (2023). https://doi.org/10.3390/aerospace10030292.
- 36. Kim, H.-S., Oh, S., Choi, J.-Y.: Quasi-1D analysis and performance estimation of a sub-scale RBCC engine with chemical equilibrium. Aerosp. Sci. Technol. 69, 39-47 (2017). https://doi.org/10.1016/j.ast.2017.06.019.
- 37. Kim, H.-S., Kim, K.-S., Oh, S.-J., Choi, J.-Y., Yang, W.-S.: A preliminary design of flight test conditions for a sub-scale RBCC engine using a sounding rocket. Int. J. Aeronaut. Space Sci. 16, 529-536 (2015). https://doi.org/10.5139/IJASS.2015.16.4.529.
- 38. Menter, F.R.: Two-equation eddy-viscosity turbulence models for engineering applications. AIAA Journal. 32, 1598-1605 (1994). https://doi.org/10.2514/3.12149.
- 39. Wilcox, D.C.: Formulation of the kw turbulence model revisited. AIAA journal. 46, 2823-2838 (2008). https://doi.org/10.2514/1.36541.

HiSST-2025-XXXX Page |

- 40. Launder, B.E., Spalding, D.B.: The numerical computation of turbulent flows. Numerical prediction of flow, heat transfer, turbulence and combustion, pp. 96-116. Elsevier (1983).
- 41. Jachimowski, C.J.: An analytical study of the hydrogen-air reaction mechanism with application to scramjet combustion. (1988).
- 42. Kartha, A., Subbareddy, P.K., Candler, G.V.: Les of subsonic reacting mixing layers. Flow Turbul. Combust. 104, 947-976 (2020). https://doi.org/10.1007/s10494-019-00066-4.
- 43. Peterson, D.M., Hassan, E.A., Bornhoft, B.J.: Improved Delayed Detached-eddy Simulation of a Round Supersonic Combustor with and without Periodic Boundary Conditions. AIAA SCITECH 2022 Forum, 2251 (2022). https://doi.org/10.2514/6.2022-2251.
- 44. Burrows, M.C., Kurkov, A.P.: An analytical and experimental study of supersonic combustion of hydrogen in vitiated air stream. AIAA Journal. 11, 1217-1218 (1973).
- 45. Waidmann, W., Alff, F., Brummund, U., Böhm, M., Clauss, W., Oschwald, M.: Experimental investigation of the combustion process in a supersonic combustion ramjet (SCRAMJET). DGLR Jahrbuch. 1994, 629-638 (1994).
- 46. Berglund, M., Wikström, N., Fureby, C.: Numerical simulation of scramjet combustion. Swedish defence research agency2005.
- 47. Oevermann, M.: Numerical investigation of turbulent hydrogen combustion in a SCRAMJET using flamelet modeling. Aerosp. Sci. Technol. 4, 463-480 (2000). https://doi.org/10.1016/S1270-9638(00)01070-1.

HiSST-2025-XXXX Page | 11